Iranian Journal of Chemical Engineering
Journal Homepage: www.ijche.com
pISSN: 1735-5397
eISSN: 2008-2355

CFD-Based Scale-Up Analysis of Airlift Photobioreactors: Effects of Superficial Gas Velocity on Hydrodynamics and Mass Transfer

Mir Mehrshad Emamshoushtari [1], Farshid Pajoum Shariati [1], Omid Tavakoli [2]*, Michael Harasek [3], Bahram Haddadi Sisakht [3]

[1] Department of Chemical Engineering, SR.C, Islamic Azad University, Tehran, Iran
[2] School of Chemical Engineering, College of Engineering, University of Tehran, Tehran, 14176, Iran
[3] Institute of Chemical, Environmental and Bioscience Engineering, TU Wien, Vienna, Austria

ARTICLE INFO

Article type:
Research article

Article history:
Received: 2026-05-16
Revised: 2026-06-04
Accepted: 2026-06-20
Available online: 2026-06-22

Keywords:
Hydrodynamics,
CFD Eulerian simulation,
Airlift reactors,
Volumetric mass transfer coefficient

ABSTRACT

Maintaining a constant superficial gas velocity (U_{sg}) is the most common criterion for scaling aerated photobioreactors, yet whether it preserves gas–liquid hydrodynamics is rarely tested directly. Euler–Euler CFD was used to characterize two baffled airlift reactors, a 9.7 L laboratory unit and a 106 L scaled-up unit, over the U_{sg} = 0.025–0.10 m·s⁻¹, evaluating gas holdup, the gas-phase velocity, and the volumetric mass transfer coefficient (k_La) alongside the Reynolds number, Froude number, and power input per unit volume (P/V). Across this range, gas holdup rose 2.4–2.6-fold and k_La rose 1.3–1.6-fold in both reactors, but the mean gas velocity increased more in the larger unit (1.4-fold vs. 1.1-fold). The extended-range simulations of the large reactor showed continued but progressively less proportional gains. The Froude number was not conserved across scales, and P/V remained consistently higher in the larger reactor. These results show that U_{sg} alone is an insufficient scale-up criterion, gas holdup, the k_La, Froude number, and P/V should be evaluated jointly.

DOI: 10.22034/ijche.2026.590277.1603 URL: https://www.ijche.com/article_248302.html

1. Introduction

Bioreactors and photobioreactors (PBRs) are closed cultivation systems that provide the controlled environment required to grow microalgae efficiently, and they are the operational units that ultimately determines whether microalgal processes can be realized on a commercial scale [1]. The performance of a PBR is governed primarily by its engineering rather than by the organism: light delivery, carbon dioxide supply, mixing, and gas–liquid mass transfer are all controlled by the reactor's hydrodynamics, so geometry, aeration, and flow behavior set the achievable growth and

*Corresponding author: otavakoli@ut.ac.ir

transfer rates [2]. Despite decades of development, scaling a PBR from laboratory to production size remains a central obstacle to its industrial adoption, because maintaining the hydrodynamic and mass-transfer conditions that favor productivity is difficult as the reactor volume increases. Therefore, the gas–liquid behavior at the scale of reactors emerges as a key engineering challenge in the design and scale-up of photobioreactors [3].

Among the vertical column configurations, airlift PBRs are widely regarded suitable for microalgal cultivation, since pneumatic gas injection provides mixing and gas–liquid contact without moving parts, typically at lower shear stress and mechanical complexity than the same in mechanically stirred systems. Aeration at the base establishes a gas-holdup difference, and hence a bulk-density difference, between the aerated riser and the less-aerated downcomer, which drives internal liquid circulation without mechanical agitation [4]. These features have made airlift and related pneumatically agitated reactors a common choice for shear-sensitive cultures, although their relative performance depends strongly on geometry and operating conditions and is not uniformly superior to that of other column reactors [5]. Among the resulting hydrodynamic descriptors, gas holdup (ε_g) is particularly important: it quantifies the fraction of dispersed gas retained in the liquid and therefore sets the gas–liquid interfacial area available for mass transfer, while also governing the liquid circulation and mixing on which the performance of the reactor depends [6]. Aeration at the base establishes a gas-holdup difference, and hence a bulk-density difference, between the aerated riser and the less-aerated downcomer, which drives internal liquid circulation without any moving parts. This circulation enhances CO_2 transfer and nutrient distribution, disperses the injected bubbles, and cycles the suspended cells between higher- and lower-irradiance regions, producing the intermittent light–dark exposure that can benefit photosynthetic growth. Because all of these functions are governed by the gas–liquid flow, hydrodynamic descriptors such as gas holdup, gas-phase velocity, liquid circulation intensity, and the volumetric mass transfer coefficient (k_La) determine the performance of the reactor and must be characterized and controlled during both design and scale-up [7–9].

Using computational fluid dynamics (CFD) has become an effective approach for analyzing gas–liquid hydrodynamics in airlift photobioreactors because it resolves the spatial distribution of gas holdup, velocity fields, and circulation patterns that are difficult to obtain experimentally. Euler–Euler multiphase models are particularly suitable for engineering simulations of bubbly gas–liquid systems, since they treat both phases as interpenetrating continua at reasonable computational cost. In previous CFD studies of airlift photobioreactors and bioreactors, Eulerian multiphase frameworks have been used to predict gas distribution, liquid circulation, and the hydrodynamics related to mass transfer, including the characteristic concentration of the gas phase in the riser relative to the downcomer [10,11]. More recent work has shown that CFD can further support the design and optimization of microalgal cultivation systems by quantifying how the geometry, sparger configuration, and internal structures of reactors affect the flow behavior and transport associated with cultivation [12,13].

Scaling- up airlift photobioreactors remains challenging because hydrodynamic and mass-transfer parameters do not necessarily change proportionally with reactor size. Increasing the superficial gas velocity (U_{sg}) generally enhances the gas holdup, liquid circulation, and mass transfer within a given reactor, however, the holdup and transfer obtained at a particular U_{sg} also depend on the geometry, gas residence time and sparger configuration of the reactor, and how the injected gas is distributed across the reactor cross-section and between the riser and downcomer. Previous scale-up studies have shown that gas holdup and oxygen transfer can differ substantially between geometrically related airlift reactors operated under comparable conditions, indicating that holding a single operating variable constant is insufficient to preserve hydrodynamic similarity [14–17]. Reliable scale-up therefore requires evaluating not only U_{sg} but also scale-dependent indicators such as gas holdup, liquid circulation, the volumetric mass transfer coefficient (k_La), and the power input per unit volume [18]. Table 1 summarizes representative studies on hydrodynamics, CFD modelling, and the scale-up of airlift (photo)bioreactors.

Table 1.
Summary of airlift bioreactor hydrodynamics, CFD, and scale-up studies.

Reactor	Method	Scale	Main parameter	Key finding	Ref.
Internal-loop airlift	Experimental	Multiple scales	Gas holdup, liquid circulation	Reactor scale directly influences hydrodynamic behavior	[19]
Internal-loop airlift	CFD	Three different scales	Riser/ downcomer gas holdup	Gas holdup increases using Euler-Euler CFD method	[14]
Airlift column photobioreactor	CFD	Single PBR geometry	Gas holdup, velocity, shear	Gas phase concentrated the riser, while downcomer gas fraction was much lower	[10]
Airlift column photobioreactor	CFD	Gas-liquid-solid system	Multiphase hydrodynamics	Euler-Euler model was able to simulate the transport precisely	[20]
Internal and external loop airlift reactors	Experimental	Internal and external configurations	Gas holdup, liquid velocity, and O_2 transfer	The reactor's hydrodynamics strongly affected all parameters	[21]
Bubble column with draft tube	Experimental	Draft-tube system	Gas holdup, k_La	U_{sg} increased gas holdup and k_La	[22]
Internal airlift reactor and bubble column	CFD	Comparative reactor geometries	Hydrodynamics, mass transfer	CFD was used to compare gas–liquid behavior and mass transfer in pneumatic reactors.	[23]
Gas–liquid internal-loop airlift reactor	Experimental and CFD	Internal-loop reactor	Local hydrodynamics	CFD and measurements were combined to characterize local gas–liquid behavior.	[24]
Cylindrical split airlift column	Experimental	Local axial/radial measurements	Local gas holdup	Gas holdup varied spatially with position and gas velocity.	[25]
Two-stage internal-loop airlift reactor	CFD	Modified internal-loop geometry	Gas holdup, velocity, mixing	Internal structural modification improved gas–liquid hydrodynamics.	[12]
Open-tube airlift photobioreactor	Experimental and CFD	Laboratory-scale open-tube, closed-tube, and wall-type configurations	Gas holdup, circulation uniformity, k_La, CO_2 capture, nutrient removal	Open-tube geometry improved hydrodynamic performance and mass transfer, the CFD model showed good agreement with experiments.	[26]

Although the effects of the scale in airlift reactors have been studied experimentally and, in some cases, numerically, systematic CFD investigations that quantitatively evaluate the combined influence of the scale of reactors on hydrodynamic, mass transfer, and similarity parameters under identical superficial gas velocities remain limited, and the relative diagnostic value of the common dimensionless and energy-based scale-up criteria (Reynolds number, Froude number, and power input per unit volume) has rarely been assessed. Therefore, the present study employs Euler–Euler CFD simulations to investigate the scale-dependent hydrodynamic and gas–liquid mass transfer behavior of two geometrically similar airlift reactors. Accordingly, the objectives of this study are threefold: (i) to quantify how the scale of reactors affects the gas holdup, gas-phase velocity distribution, and volumetric mass transfer coefficient ($k_L a$) at the identical superficial gas velocity; (ii) to assess, over an extended aeration range for the larger reactor, whether increasing U_{sg} can compensate for the scale-dependent reductions; and (iii) to evaluate the Reynolds number, Froude number, and power input per unit volume as similarity indicators and their relative diagnostic value. Furthermore, the Reynolds number, Froude number, and power input per unit volume are evaluated to provide a comprehensive assessment of hydrodynamic similarity. By integrating these hydrodynamic, mass transfer, and dimensionless criteria within a single CFD framework, the suitability of superficial gas velocity as a scale-up criterion is evaluated in this study and potentially more reliable indicators for the CFD-assisted design and scale-up of airlift photobioreactors are identified.

The novelty of this study therefore lies not in reporting that superficial gas velocity alone is not sufficient, which is a conclusion that has been established in the literature, but in the integrated evaluation of hydrodynamic, mass transfer, and dimensionless and energy-based similarity criteria in a single CFD framework for two geometrically similar baffled airlift photobioreactors, a configuration and combined analysis that have received little attention in previous scale-up studies. On this basis, the contribution of this work is threefold. First, it presents a CFD investigation of geometrically similar baffled airlift photobioreactors for microalgal CO_2 capture, a configuration that has received limited attention compared with cylindrical internal-loop and concentric-tube airlift reactors. Second, it develops a CFD-derived engineering correlation between the $k_L a$ and gas holdup for the geometry of the investigated reactor, together with an explicit statement of the range and limitations of its applicability. Third, it provides a quantitative comparison of the Reynolds number, Froude number, and power input per unit volume as similarity indicators, showing that among the examined criteria the Froude number provides the most informative indication of scale-dependent hydrodynamic similarity.

2. Materials and Methods

2.1. Geometry

Two airlift reactors of different scales were used in this study: a small reactor and a large reactor. The small reactor had dimensions of 18.5 cm × 15 cm × 45 cm, corresponding to a total volume of approximately 12.5 L. During operation, the reactor was filled to a height of 35 cm of the liquid, resulting in a working volume of approximately 9.7 L. The large reactor had dimensions of 90 cm × 50 cm × 25 cm, giving a total volume of approximately 112.5 L. This reactor was operated at a height of 85 cm of the liquid, corresponding to a working volume of approximately 106 L.

In each reactor, two internal baffles were installed to establish the airlift configuration. For the small reactor, each baffle had a thickness of 1 cm, a width of 15 cm, and a height of 26.5 cm. In the large reactor, the baffles had the same thickness of 1 cm and width of 25 cm, but a height of 75 cm. In both reactors, the baffles were positioned 5 cm above the reactor bottom. Aeration was provided using a circular showerhead-type sparger with a diameter of 5 cm, positioned centrally in the reactor at 1 cm above the bottom. The schematic of the airlift reactor along with its larger scale is presented in Figure 1.

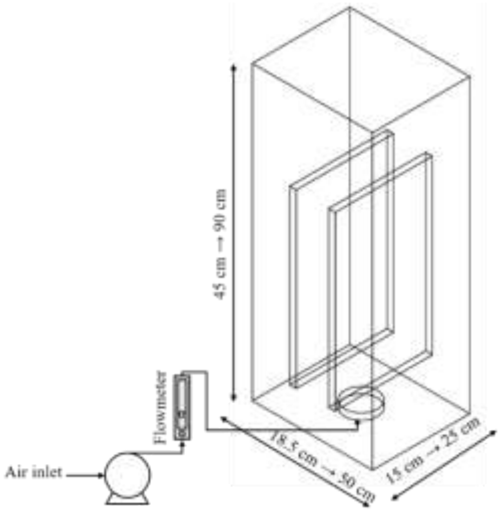

Figure 1. Schematics of the airlift reactor used in this study along with its larger variation.

Table 2 presents the comparison between the performance and accuracy of different mesh cell sizes.

2.2. Mesh generation

The geometry of both small and large reactors was built in ANSYS DesignModeler (2025 R2), and the corresponding computational grids were generated in ANSYS Meshing. Boundary conditions were assigned as follows: the sparger surface was treated as a velocity inlet through which the determined superficial gas velocities were imposed; the free surface at the top of the column was set as a pressure outlet held at atmospheric pressure; and all remaining surfaces were defined as solid walls. At these walls, the liquid obeyed a no-slip condition, whereas the gas phase was permitted to slip freely. The domain was discretized with an unstructured tetrahedral mesh at a nominal element size of 3 mm. This resolution followed the Eulerian requirement that the cell dimension exceed roughly twice the bubble diameter; with a 1 mm bubble assumed in this work, a 3 mm cell satisfied that constraint while keeping the element count tractable [26].

Table 2.
Comparison between different mesh cell sizes

Nominal element size (mm)	Number of elements	Relative error of liquid height (%)	Approximate computation time
5	~ 300,000	6.9	1 – 2 days
3	~ 1,000,000	1.8	3 – 4 days
2	~ 3,000,000	−	~ 6 days

2.3. CFD simulation

All computations were carried out in ANSYS Fluent 2025 R2, and executed in parallel on a four-core workstation clocked at 3.70 GHz. As noted above, a Eulerian–Eulerian two-fluid description was adopted because the air–water mixture operated in the bubbly regime and the objective was the bulk hydrodynamic response to the aeration rather than the trajectories of individual bubbles. Turbulence was closed with the standard k–ε model, a common choice in airlift studies at this scale owing to its robustness and its reliable prediction of mean-flow quantities [27]. Momentum coupling between the phases combined drag [28], virtual-mass [29], and lift [30] contributions. Water was assigned as the continuous phase and air as the dispersed phase, the latter represented by a uniform mean bubble diameter of 1 mm. A single representative bubble diameter was prescribed as a resolved bubble size distribution, which is aligned with the monodisperse Euler–Euler method widely used for engineering-scale simulations of airlift and bubble column reactors, where the objective is the bulk hydrodynamic response instead of the dynamics of individual bubbles. The 1 mm value was taken as the representative of the bubbles generated at the perforated showerhead sparger in the near-injection region. Since identical values were applied at both small and large reactors, this assumption is common to the small and large systems and does not bias the scale-to-scale comparison that is the focus of this study.

The system operated at 101.325 kPa, and pressure–velocity coupling was handled with the SIMPLEC scheme [31]. Each case was advanced in time using a fixed step of 0.01 s with up to 70 inner iterations per step, and convergence was enforced by driving all scaled residuals below 1×10^{-5}. A total physical time of 15 s proved sufficient for the flow to settle into a pseudo-steady state, identified by the stationary values of the overall gas holdup and the circulating liquid velocity. These converged fields, together with the velocity data sampled at fixed monitoring points, were then used to characterize the internal circulation. Because each simulation was deterministic and run at a fixed operating point, no replicate-based statistical treatment was applied. The predictive capability of this modeling approach for the airlift photobioreactors of comparable scale has been established previously through direct comparison with experimental data [26], and a validation specific to the present geometry is presented in Section 3.1.

2.4. Grid independence

Mesh sensitivity was assessed to confirm that the reported results were independent of grid resolution while keeping the computational cost reasonable. Alongside the 3 mm baseline, a coarser (5 mm) and a finer (2 mm) element size were evaluated for comparison.

2.5. Dimensionless and energy-based scale-up parameters

To support the scale-up analysis, the dimensionless and energy-based parameters were calculated for both reactor scales. The Reynolds number (*Re*) was used to evaluate the relative importance of inertial and viscous forces, whereas the Froude number (*Fr*) was used to measure the balance between inertial and gravitational effects. In addition, the power input per unit volume (*P/V*) was estimated as an energy-based indicator of aeration intensity. These parameters were selected to provide a systematic basis for comparing the hydrodynamic similarity of the small and large airlift reactors under identical superficial gas velocities. The Reynolds and Froude numbers were calculated according to equations (1) and (2) respectively:

$$Re = \frac{\rho_l U_{sg} H_L}{\mu_l} \quad (1)$$

$$Fr = \frac{U_{sg}^2}{g H_L} \quad (2)$$

where ρ_l is the density of the liquid, μ_l is the dynamic viscosity of the liquid, U_{sg} is the superficial gas velocity, and g is the gravitational acceleration. The operating height of the liquid, H_L, was selected as the characteristic length because the present scale-up analysis focuses on vertical gas transport, hydrostatic pressure effects, and buoyancy-driven circulation within the airlift reactors. The pneumatic power input per unit volume was estimated using a hydrostatic pressure-based formulation, as expressed in equation (3):

$$\frac{P}{V} = \rho_l g U_{sg} \ln\left(\frac{P_b}{P_t}\right) \quad (3)$$

where P_b and P_t are the pressures at the sparger location and at the top of the liquid column respectively. The top pressure was assumed to be atmospheric pressure, while the pressure at the sparger was estimated from the hydrostatic liquid head according to equation (4):

$$P_b = P_t + \rho_l g H_L \quad (4)$$

This formulation accounts for the influence of height of the liquid on the pneumatic energy required for gas injection and was therefore used to compare the aeration intensity between the small and large airlift reactors.

3. Results and discussion

3.1. Effect of superficial gas velocity on gas holdup

Before analyzing the scale-dependent behavior, the CFD model was validated against experimental data to establish its predictive reliability. The Euler-Euler method, turbulence closure, and interphase closures used here follow those previously validated against experimental hydrodynamic and mass transfer measurements for airlift photobioreactors of comparable scale and operating regime [26]. To provide a direct validation for the present configuration, the overall gas holdup predicted by CFD for the small reactor was compared with experimental measurements over the superficial gas velocity range of 0.025 – 0.10 m.s^{-1}, as shown in Figure 3. The simulated gas holdup increased monotonically with U_{sg} and reproduced the experimentally observed trend, with a maximum deviation of approximately ۴,۲% and a mean absolute deviation of approximately 4%. This level of agreement confirms that the model adequately captures both the magnitude and the aeration-rate dependence of the gas-phase distribution in the baffled airlift geometry. Because experimental data were available only for the small reactor, the validated model was subsequently applied to the large (106 L) reactor; the results corresponding to large reactors are therefore presented as predictions of an experimentally validated model rather than as directly measured quantities. Given the consistency of the modeling approach across both scales and its prior experimental validation in related work [26], the model is considered suitable for the comparative scale-up analysis that follows. In this study, the variation of gas holdup with superficial gas velocity was examined for both the small and large airlift reactors to assess how scale of reactors affects gas-phase distribution. The volume fraction of air is shown in Figure 2 (a, b) and the results of gas holdup at different U_{sg} are presented in Figure 3.

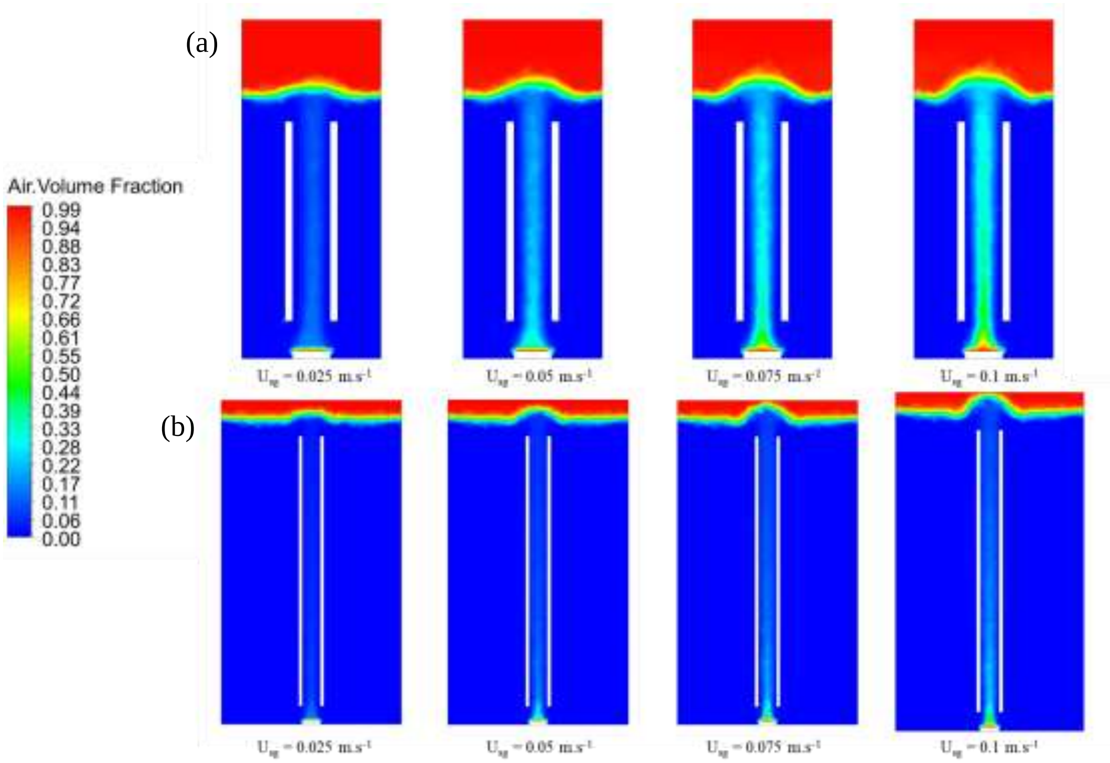

Figure 2. Air volume fraction of contour for (a) small reactors, (b) large reactors.

The simulated air volume fraction contours provide further insight into the internal gas distribution responsible for the observed gas holdup behavior. As shown in Figure 2 (a, b), in both reactors the gas phase was mainly concentrated in the central riser region above the sparger, while the downcomer zones remained dominated by the liquid phase. Increasing U_{sg} from 0.025 to 0.1 m.s^{-1} intensified the gas bubbles and increased the local air volume fraction in the riser, showing that a larger number of bubbles were transported upward through the central section of the reactor. This behavior confirms that the riser acted as the main gas-liquid contact region, whereas the baffles effectively separated the aerated riser from the less-aerated down comer region. A clear difference between the two small and large reactors can also be observed from the contours. In the small airlift reactor, the gas cloud occupied a relatively wider portion of the riser and showed stronger horizontal spreading as the superficial gas velocity increased. This wider gas dispersion resulted in a more pronounced accumulation of gas within the reactor and is consistent with the higher values of the overall gas holdup reported for the small system. In contrast, the large airlift reactor showed a narrower and more vertically extended gas cloud, particularly at lower superficial gas velocities. Although the gas cloud become stronger at higher aeration rates, the gas phase remained more limited around the central sparger axis and occupied a smaller fraction of the total liquid volume. This explains why the large airlift reactor showed considerably lower average gas holdup despite being operated at the same superficial gas velocities. The contour results therefore demonstrate that scale-up changed not only the magnitude of gas holdup but also the spatial distribution of the dispersed gas phase. In the larger reactor, the injected air was distributed over a substantially larger liquid volume and a longer flow path, reducing the average gas volume fraction within the reactor. Moreover, the more limited gas cloud suggests weaker radial gas dispersion and less effective gas distribution across the reactor cross-section.

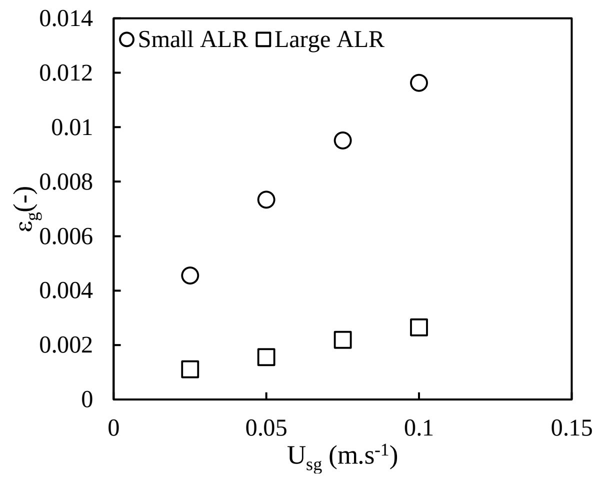

Figure 3. Gas holdup vs. superficial gas velocity across small and large reactors.

As shown in Figure 3, the overall gas holdup in both reactors increased by increasing superficial gas velocity, indicating that higher aeration rates raised the fraction of the dispersed gas retained within the liquid phase. For the small airlift reactor, ε_g increased from approximately 0.0045 at the U_{sg} = 0.025 m.s^{-1} to about 0.0116 at the U_{sg} = 0.10 m.s^{-1}. A similar increasing trend was observed in the large airlift reactor; however, the corresponding gas holdup values were considerably lower, rising only from almost 0.0011 to 0.0026 over the same superficial gas velocity range. This shows, that although increasing U_{sg} enhances the gas holdup in both reactors, the magnitude of gas holdup has been strongly affected by reactor scale. Basically, at identical superficial gas velocities, the small airlift reactor maintained nearly four to five times higher gas holdup than the large airlift reactor, showing that the gas-liquid distribution was not preserved during scale-up when U_{sg} was the only parameter that was kept constant. The observed gas holdup behavior is consistent with previous experimental and numerical studies on airlift reactors. Blažej et al. reported that gas holdup increased by increasing the input gas velocity in internal-loop airlift reactors and showed that the values of reactors can significantly influence hydrodynamic parameters, confirming that gas holdup is not governed by superficial gas velocity alone [19]. Similarly, Davarnejad et al. used CFD to investigate internal-loop airlift reactors at different scales and showed that gas holdup in both the riser and downcomer increased with superficial gas velocity, supporting the monotonic trend observed in the present simulations [14]. The spatial distribution of the gas phase shown by the air volume fraction contours also agrees with earlier studies, which demonstrate that gas holdup is strongly affected by reactor geometry and varies locally within the riser and downcomer regions [32].

3.2. Effect of superficial gas velocity on average air velocity

The air velocity contours achieved by the simulation were first analyzed to describe the spatial structure of gas-phase transport in the small and large airlift reactors. As shown in Figure 4 (a, b), the highest air velocities were concentrated in the central riser region immediately above the sparger, where the injected air formed a distinct upward-moving gas cloud between the internal baffles. However, the regions outside the baffles showed substantially lower air velocities, indicating that the gas-phase motion was mainly restricted to the aerated riser, while the downcomer zones remained predominantly liquid-dominated. As the superficial gas velocity increased from 0.025 to 0.10 m.s^{-1}, the high-velocity region became more intense and extended over a larger portion of the riser height, confirming that higher aeration rates increased the upward momentum of the dispersed gas phase. This flow structure is consistent with the typical operating mechanism of airlift reactors, where gas injection produces a density difference between the riser and downcomer regions and thus drives internal circulation.

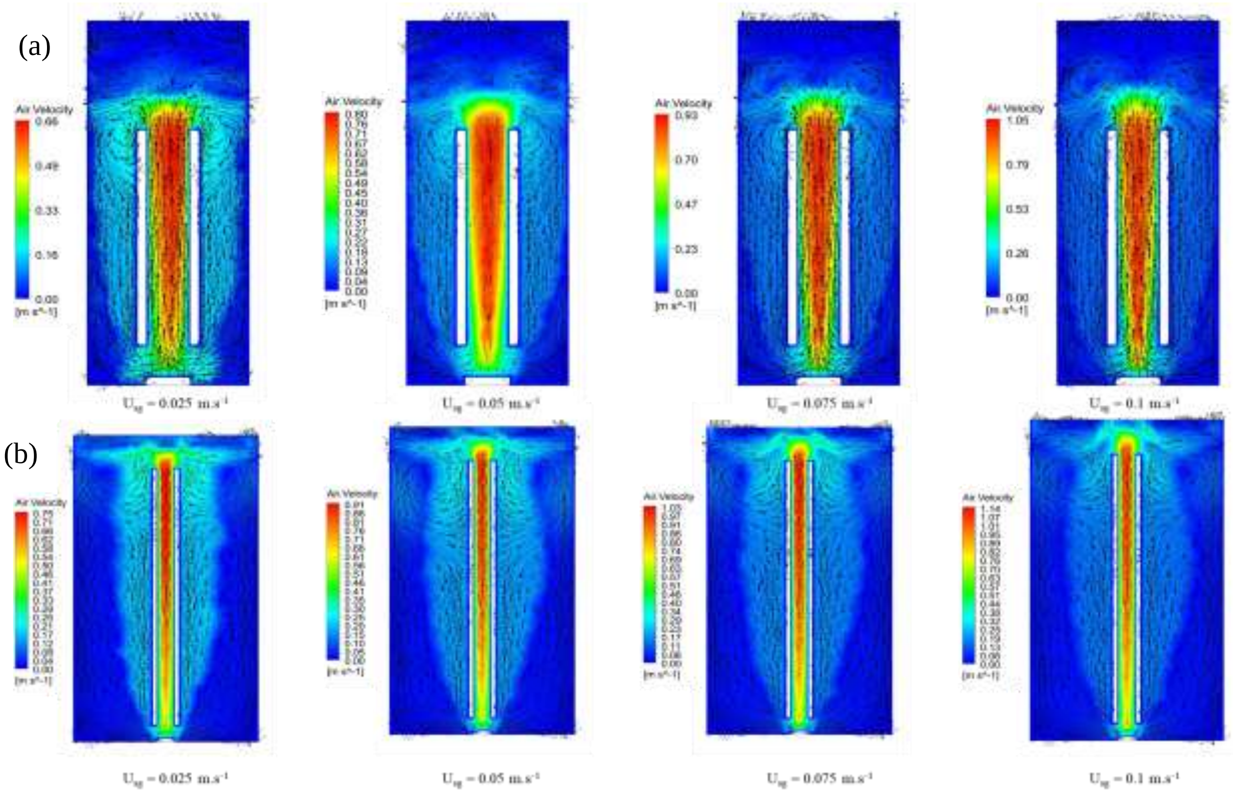

Figure 4. Air velocity contours for (a) small airlift reactors, (b) large airlift reactors.

The air velocity contours also reveal clear scale-dependent differences in the gas-phase velocity field. In the small airlift reactor, the high-velocity region occupied a relatively broad portion of the riser and showed noticeable lateral spreading between the baffles, particularly at higher superficial gas velocities. This indicates that the injected gas was more effectively distributed across the riser cross-section, promoting stronger gas–liquid contact within the aerated zone. By contrast, in the large airlift reactor, the high-velocity region appeared narrower and more vertically confined along the central axis above the sparger. Although increasing U_{sg} intensified the cloud in the large reactor, the gas-phase motion remained concentrated in a limited region of the riser rather than spreading uniformly across the reactor width. This suggests that the scale of reactors influenced the spatial distribution of gas momentum, with the larger geometry producing a more localized gas jet and weaker radial dispersion compared with the small systems. The quantitative variation of average air velocity with superficial gas velocity is shown in Figure 5. In both reactors, the average air velocity increased as U_{sg} increased from 0.025 to 0.10 $m.s^{-1}$, confirming that higher aeration rates enhanced the overall gas-phase transport through the reactor. In the small airlift reactor, the average air velocity increased from approximately 0.124 m.s^{-1} at the U_{sg} = 0.025 m.s^{-1} to about 0.141 m.s^{-1} at the U_{sg} = 0.10 m.s^{-1}. For the large airlift reactor, the corresponding values increased from approximately 0.095 to 0.130 m.s^{-1} over the same range. Although the small airlift reactor maintained higher average air velocities at all superficial gas velocities, the difference between the two scales was less pronounced than what was observed for gas holdup. This indicates that scale-up had a stronger effect on gas holdup than on the mean upward gas velocity, suggesting that the injected gas in the large reactor was transported upward at relatively comparable velocities but was retained less effectively within the liquid phase.

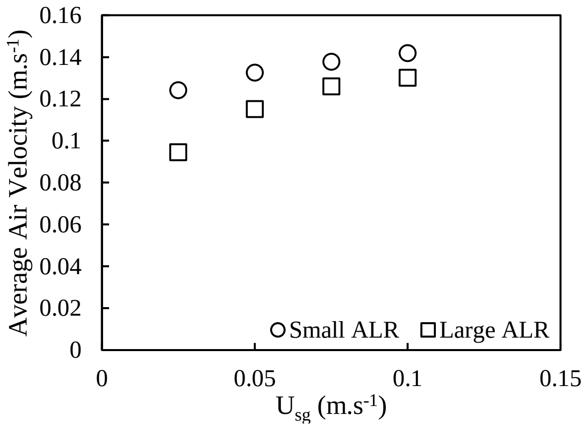

Figure 5. Air-phase velocity vs. superficial gas velocity across small and large reactors.

Overall, the air velocity results demonstrate that increasing the superficial gas velocity enhances the gas-phase transport in both small and large reactors, however, the resulting velocity field is not fully scale-independent. Although the large airlift reactor produced average air velocities relatively close to those obtained in the small airlift reactor, its gas holdup remained substantially lower. This indicates that the gas phase in the large reactor was transported upward through the riser at comparable mean velocities, but with reduced retention and weaker spatial dispersion within the liquid volume. Therefore, the lower gas holdup observed in the large airlift reactor cannot be attributed solely to the reduced gas-phase velocity, but rather to the scale-dependent changes in gas residence and distribution. These findings further confirm that maintaining identical superficial gas velocity is insufficient to ensure complete hydrodynamic similarity during scale-up, since similar average air velocities may still be associated with markedly different gas holdup and gas distribution patterns.

3.3. Volumetric mass transfer coefficient (k_La)

The volumetric mass transfer coefficient (k_La) is one of the main performance indicators in airlift photobioreactors because it describes the overall capacity of the system to transfer the components of the gas-phase into the liquid phase. For instance, in microalgal systems, efficient gas-liquid mass transfer is essential for maintaining sufficient CO_2 availability, promoting photosynthetic carbon fixation, and supporting stable reactor operation. Since k_La is strongly influenced by hydrodynamic conditions, its variation provides a useful link between the simulated flow behavior and the expected biological performance of the reactor. Figure 6 represents a comparison of k_La between small and large airlift reactors.

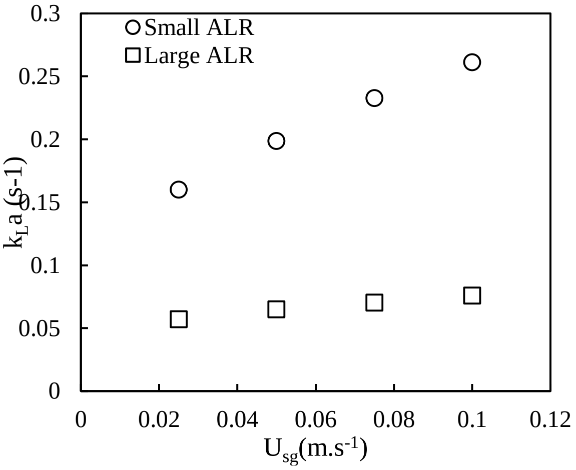

Figure 6. Comparison of k_La between small and large airlift reactors.

As observed, the small airlift reactor's k_La increased constantly by increasing superficial gas velocity, showing improved gas-liquid mass transfer under high aeration conditions. As U_{sg} increased from 0.025 to 0.10 m.s^{-1}, k_La rose from approximately 0.16 s^{-1} to about 0.26 s^{-1}. This enhancement can be because of the combined effects of the increased gas holdup, stronger bubble dispersion, and greater gas-liquid interfacial area within the riser. At higher aeration rates, the larger number of bubbles introduced to the reactor increased the available contact surface between the gas and liquid phases, while the intensified upward gas motion promoted stronger mixing and the renewal of the liquid film around the bubbles. Consequently, the resistance to gas transfer was reduced and the overall volumetric mass transfer capacity of the small airlift reactor was improved.

As for the large airlift reactor, k_La increased by increasing U_{sg}, however, the absolute values were considerably lower than those obtained in the small airlift reactor. As U_{sg} increased from 0.025 to 0.10 m.s^{-1}, k_La increased only from approximately 0.057 s^{-1} to 0.075 s^{-1}. This shows that the higher aeration improved the mass transfer capacity of the large reactor, but the enhancement was limited compared with the same of the small system. At identical superficial gas velocities, the k_La values in the small airlift reactor were approximately three times higher than those in the large airlift reactor. This difference is consistent with the gas holdup results discussed earlier, where the large airlift reactor showed substantially lower gas holdup and a more confined gas cloud. Since k_La depends greatly on the gas-liquid interfacial area and bubble residence within the liquid phase, the reduced gas holdup in the large reactor directly limited its volumetric mass transfer performance.

The scale-dependent reduction in k_La has important effects for the scale-up of airlift photobioreactors. Although increasing U_{sg} improved mass transfer in both reactors, operating the large airlift reactor at the same superficial gas velocity did not reproduce the mass transfer performance of the small airlift reactor. This behavior can be because of the lower gas holdup and more localized gas cloud observed in the large reactor, which reduced the effective gas–liquid interfacial area and limited bubble residence within the liquid phase. As a result, the larger reactor showed weaker volumetric mass transfer despite receiving the same insignificant gas velocity. Since gas holdup governs the available gas–liquid interfacial area, the CFD results from both small and large reactors were combined to develop an empirical correlation relating the volumetric mass transfer coefficient to the overall gas holdup. Regression of all simulated data yielded:

$$k_La = 6.16\varepsilon_g^{0.706}, R^2 = 0.98 \quad (5)$$

Furthermore, Figure 7 compares the k_La values predicted by CFD with those calculated from the correlation. Most data points fall within the ±25% deviation lines, indicating that the proposed equation provides a satisfactory representation of the simulated results over the investigated operating range. The exponent of 0.706 suggests the sub-linear dependence of mass transfer on gas holdup, implying that the increases in gas retention continue to enhance mass transfer but by diminishing returns. The correlation may therefore serve as a practical engineering relationship for estimating $k_L a$ from CFD or experimentally determined gas holdup for geometrically similar airlift photobioreactors operating under the investigated conditions.

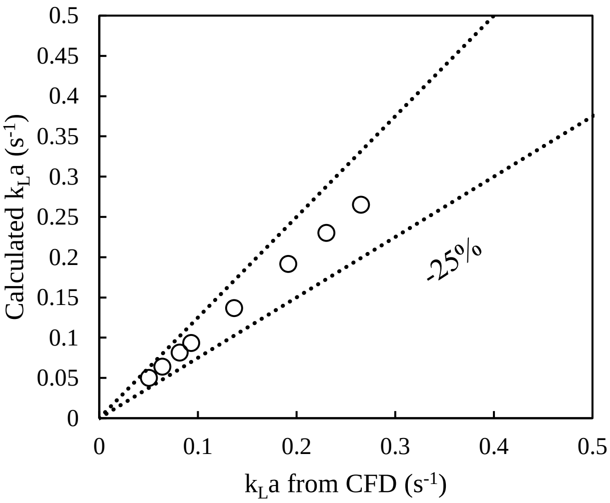

Figure 7. Comparison between the calculated $k_L a$ (s^{-1}) and the one derived from CFD

The proposed relationship further demonstrates the strong dependence of volumetric mass transfer on gas holdup, as higher gas holdup increases the effective gas–liquid interfacial area available for mass transfer. The exponent lower than unity indicates a sub-linear relationship, suggesting diminishing improvements in $k_L a$ as gas holdup increases, which is commonly due to the bubble coalescence, reduced interfacial area efficiency, and changes in flow regime at higher aeration rates. Similar nonlinear relationships between gas holdup and $k_L a$ have been reported in previous experimental studies and review articles on airlift reactors, confirming that gas holdup is one of the dominant hydrodynamic parameters controlling gas–liquid mass transfer and is widely used for developing predictive engineering correlations [33–35].

The $k_L a - \varepsilon_g$ exponents reported for airlift reactors vary widely with geometry, flow regime, and bubble-size behaviour: Blažej et al. [35] obtained about 1.1–1.4 (classical value 1.2), whereas the two-stage internal-loop airlift correlations of Zhang et al. [36] ($\varepsilon_g \propto U_g^{0.71}, k_L a \propto U_g^{0.35}$) imply $k_L a \propto \varepsilon_g^{\sim 0.5}$. The present exponent of 0.706 falls within this range, and its value is consistent with the theoretical airlift correlation of Ayazi Shamlou et al. [37]. Derived [illegible]m the penetration theory, their m[illegible]ves $k_L a \propto \varepsilon_g (1 - \varepsilon_g)^{-1.5} \cdot d_B^{-1.5} \cdot$ [illegible] $+ C_0 (U_{sg} + U_{sl})]^{0.5}$, so that due to the low gas holdups in the present study, the explicit dependence on holdup is approximately linear, while $k_L a$ is dominated by the bubble diameter ($\propto d_B^{-1.5}$) and additionally depends on holdup through the liquid circulation velocity. In real reactors the bubble diameter decreases by increasing U_{sg}, which raises the effective experimental exponent; the monodisperse fixed-diameter assumption used here removes this dominant contribution, so the fitted exponent reflects mainly the hydrodynamic and residence dependence and sits toward the lower end of the reported range. The correlation is therefore recommended as an engineering estimator for geometrically similar baffled airlift photobioreactors in the bubbly air–water regime over the fitted range ($U_{sg} = 0.025 - 0.10$ $m.s^{-1}$) and should not be extrapolated to higher aeration, where the extended-range results (Section 3.4) show the $k_L a - \varepsilon_g$ relationship flattening [36, 37]. The proposed correlation enables the rapid estimation of the volumetric mass transfer performance from gas holdup measurements or the CFD predictions without requiring separate mass-transfer simulations or experiments within the validated operating range. This makes the correlation particularly useful for the preliminary reactor design, CFD-assisted optimization, and scale-up studies of geometrically similar baffled airlift photobioreactors. It should be noted that all simulations used a single, constant bubble diameter of 1 mm, and that this assumption has a direct influence on ε_g and k_La. In real reactors the bubble size is not uniform but is set by the dynamic balance between the coalescence and breakup, which depends on the local turbulence intensity, gas fraction, and liquid properties; at higher superficial gas velocities, the intensified bubble interaction and coalescence generally shift the size distribution toward larger diameters. Nevertheless, since the identical bubble-size assumption was applied at both scales, its effect is largely systematic; the scale-dependent differences in gas holdup and k_La, which are reported here and underpin the conclusions of this study, are therefore expected to remain valid. A more rigorous treatment incorporating a population balance model (e.g., the MUSIG approach) or coupled CFD–PBM simulation to resolve the local bubble-size distribution is identified as a valuable direction for future work.

Altogether, the lower gas holdup and k_La of the large reactor can be traced to a single cause. The showerhead sparger has the same 5 cm footprint in both reactors, whereas the large reactor has a substantially larger cross section, liquid volume, and rise path; at identical superficial gas velocity the injected gas is therefore not spread over a proportionally larger area but remains concentrated as a narrow central plume, as shown by the air volume fraction and velocity contours. This limitation can be compounded by the loss of buoyancy-related similarity (the Froude number falls to 0.41 of its small-scale values) which weakens radial gas dispersion. Because the gas is distributed more thinly through the larger liquid volume, the average gas holdup is 4 to 5 times lower; and since the specific interfacial area changes with holdup, the reduction propagates directly into the almost 3-fold lower k_La. However, the average air velocity is nearly preserved across scales because, for the fixed 1 mm bubble, it is set mainly by local buoyancy rather than by reactor size. The scale-dependent penalty therefore manifests in gas holdup and spatial distribution rather than upward gas velocity, which is why gas holdup and k_La decline far more strongly than the mean air velocity between two scales.

3.4. Wide operating range and scale-dependent behavior

To examine whether the hydrodynamic improvements observed in the common operating range could be extended to higher aeration conditions, additional simulations were performed over a wider range of superficial gas velocity. The purpose of this analysis is to evaluate the broader response of the reactor in terms of gas holdup, volumetric mass transfer coefficient, and average air velocity, and to determine whether increasing U_{sg} could compensate for the scale-dependent reductions observed in the large airlift reactor. As shown in Figure 8 (a – c), all three parameters increased by increasing superficial gas velocity, confirming that higher aeration generally enhanced the gas holdup, gas-liquid mass transfer, and upward gas-phase transport. However, the results from the wide range also show that these improvements were not strictly proportional across the entire operating range, indicating that the reactor response became increasingly dependent on scale and regime at higher gas velocities.

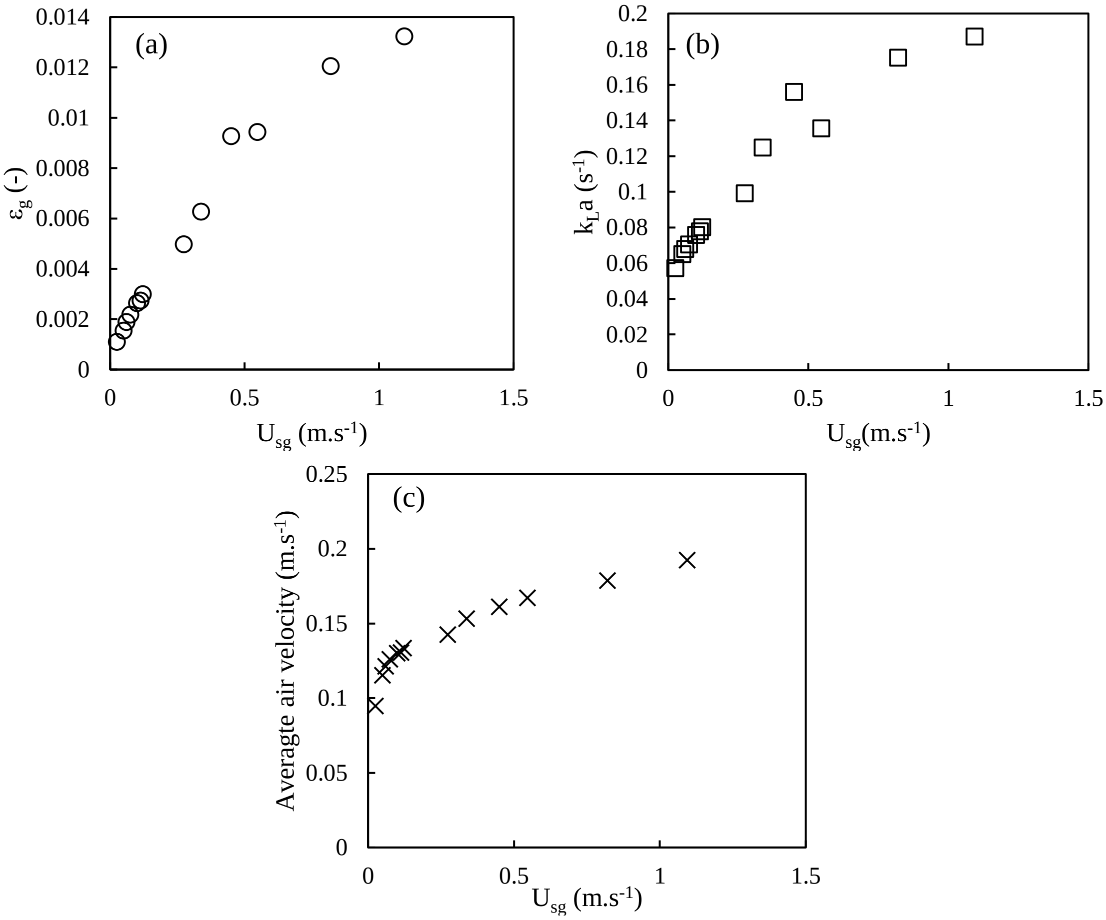

Figure 8. Behavior of the wide range of large reactors: (a) gas holdup, (b) $k_L a$, (c) air velocity.

The extended gas holdup results (Figure 8 (a)) shows that increasing superficial gas velocity continued to enhance the gas holdup over the wider operating range. As U_{sg} increased, the overall gas holdup rose from approximately 0.0011 at the lowest aeration to about 0.013 at the highest superficial gas velocity. However, the increase was not uniform across the entire range. At lower gas velocities, gas holdup increased more gradually, whereas a stronger rise was observed at intermediate aeration rates, indicating more effective bubble entrainment and gas accumulation within the reactor. At higher values of U_{sg}, the rate of increase became less pronounced, suggesting that additional aeration did not result in proportional gas retention. This behavior may be associated with intensified bubble interactions, coalescence, and faster cloud transport at elevated gas flow rates, which can reduce the effective residence of bubbles within the liquid phase despite the larger amount of gas introduced into the system. The extended $k_L a$ results (Figure 8 (b)) followed the same general trend as gas holdup, confirming that the enhanced gas holdup influences the gas-liquid mass transfer positively. As the superficial gas velocity increased across the extended range, $k_L a$ rose from approximately 0.057 s^{-1} at the lowest aeration to about 0.187 s^{-1} at the highest aeration. This increase can be due to the greater number of bubbles introduced into the reactor, which increased the available gas–liquid interfacial area and promoted more effective renewal of the liquid side around the bubbles. However, similar to the gas holdup behavior, the increase in k_La was not strictly linear over the entire operating range. At higher gas velocities, the increase in k_La became less proportional to the increase in U_{sg}, suggesting that intensified aeration may be accompanied by the stronger bubble coalescence, shorter gas residence time, and less efficient utilization of the injected gas for mass transfer.

Figure 8 (c) shows the extended average air velocity results, further confirming the non-proportional nature of the reactor response at higher aeration rates. As U_{sg} increased, the average air velocity rose from approximately 0.095 m.s^{-1} at the lowest gas velocity to about 0.19 m.s^{-1} at the highest gas velocity. However, the slope of this increase decreased at higher values of U_{sg}, indicating that the gas-phase velocity became less sensitive to additional aeration. When considered together with the gas holdup and k_La trends, this result suggests that increasing U_{sg} can partially improve hydrodynamic and mass transfer performance, but the improvement becomes progressively less efficient at higher aeration rates. Therefore, compensating for scale-dependent losses by simply increasing superficial gas velocity may not be the most effective scale-up strategy, as higher aeration can lead to reducing hydrodynamic benefits and potentially greater energy demand. These findings indicate that performance-based scale-up criteria, such as target gas holdup, target k_La, circulation intensity, or power input per unit volume, should be considered in addition to superficial gas velocity.

3.5. Scale-up analysis based on power input per volume

To evaluate the scale-up behavior more systematically, hydrodynamic similarity was further examined using dimensionless and energy-based parameters. Although superficial gas velocity is commonly used as a primary operating variable in aerated reactors, the results discussed in the previous sections showed that maintaining the same U_{sg} did not preserve gas holdup, gas-phase distribution, or k_La between the small and large airlift reactors. Therefore, additional scale-up indicators, including the Reynolds number, Froude number, and power input per unit volume, were analyzed to clarify how changes in reactor size affected the balance between inertial, gravitational, and energy-input effects. This analysis provides a more comprehensive basis for interpreting the observed scale-dependent hydrodynamic and mass transfer behavior.

The Reynolds and Froude numbers both increased by increasing superficial gas velocity, but their scale-dependent behavior was different. As shown in

Figure 9(a), the large airlift reactor showed higher Reynolds numbers than the small airlift reactor at all U_{sg} values, mainly due to its larger characteristic length. This indicates that inertial forces were dominant over viscous forces in both reactors, particularly in the large system. Therefore, the differences previously observed in gas holdup and k_La are unlikely to be associated with a transition in the flow regime, but rather with scale-dependent changes in gas distribution, the residence time, and circulation structure. In contrast,

Figure 9(b) shows that the Froude number was not preserved between the two scales. Since the Froude number represents the relative importance of inertial forces to gravitational effects, the difference between the small and large airlift reactors indicates that buoyancy-related dynamic similarity was not maintained when the same U_{sg} was applied. This is particularly important for airlift reactors, where circulation is mostly driven by the density difference between the aerated riser and the downcomer.

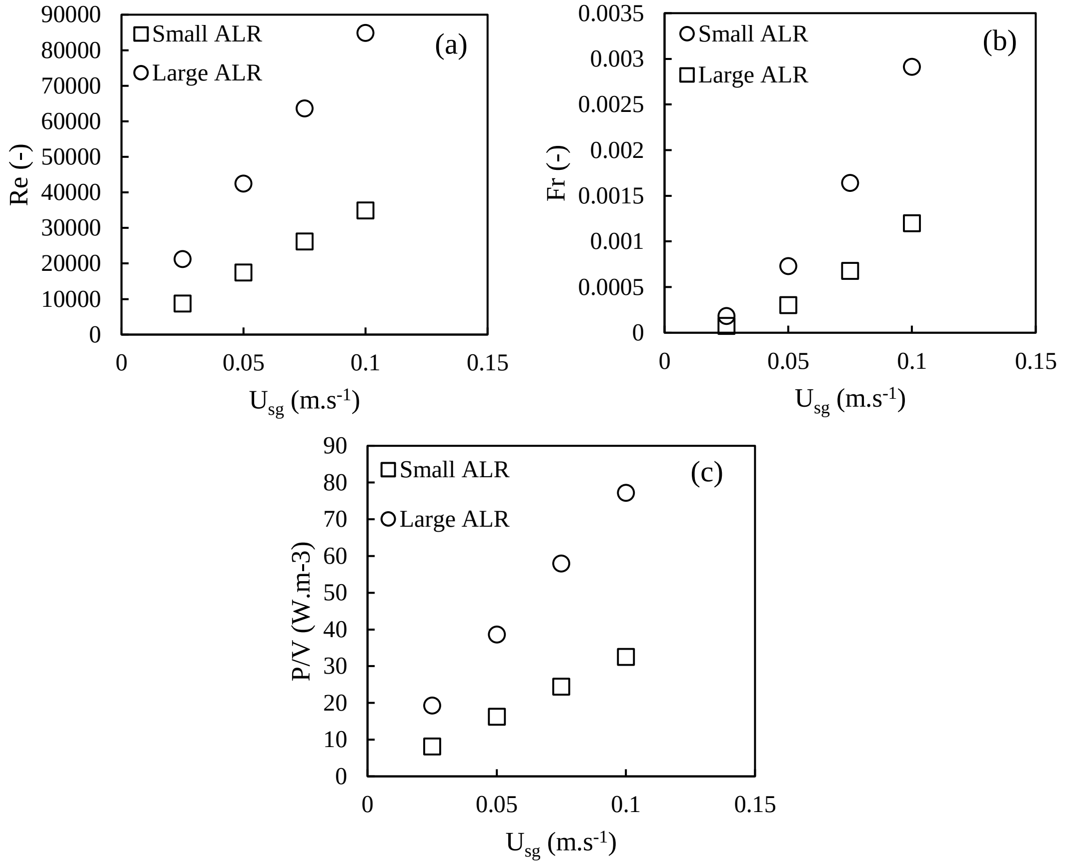

Figure 9. Hydrodynamic scale-up parameters vs. U_{sg} across reactor scales: (a) Re, (b) Fr, (c) P/V.

Power input per unit volume was further evaluated as an energy-based scale-up parameter, since pneumatic energy input governs bubble generation, gas dispersion, and liquid circulation in airlift reactors. As shown in

Figure 9(c), *P/V* increased by increasing superficial gas velocity for both small and large reactors, indicating that higher aeration rates were accompanied by greater energy input into the liquid phase. At a given *Usg*, the large airlift reactor showed higher *P/V* values than the small airlift reactor, which is due to its greater liquid height and the corresponding increase in hydrostatic pressure that must be overcome during gas injection. This result indicates that identical superficial gas velocities do not necessarily require equivalent energetic conditions across different reactor scales. Accordingly, *P/V* provides an additional basis for interpreting scale-dependent aeration requirements and reinforces the limitation of using *Usg* alone as a scale-up criterion.

Although *P/V* increased with scale according to the hydrostatic pneumatic power formulation, the large airlift reactor still showed noticeably lower gas holdup and k_La

than the small airlift reactor at identical U_{sg}. This indicates that higher energy input per unit volume does not necessarily result in the improved gas retention or mass transfer when the gas phase remains spatially confined and the effective gas–liquid contact volume is limited. In the large reactor, the injected gas formed a more localized cloud and was distributed over a larger liquid volume, which reduced the average gas volume fraction and limited the available interfacial area for mass transfer. Therefore, the scale-up behavior cannot be explained by a single parameter alone. Instead, the combined trends of *Re, Fr*, and *P/V* demonstrate that hydrodynamic similarity requires simultaneous consideration of inertial effects, buoyancy-driven circulation, gas residence, and energy input.

Because the two reactors are geometrically similar, Re, Fr, and P/V all change with the characteristic liquid height (ratio 2.43) and are therefore not independent, so their relative importance is assessed from the direction of change with scale rather than by independent variation. At a fixed superficial gas velocity, Re and P/V both increase by increasing scale (by factors of 2.43 and 2.37), where Fr decreases to 0.41 of its small-scale value. Since the gas holdup and $k_L a$ of the large reactor are lower by factors of about 4–5 and 3 respectively, the Froude number is the only parameter that changes in the same direction as the observed performance, which makes it the most diagnostic indicator of the loss of hydrodynamic similarity among the three examined. This is physically reasonable given the buoyancy-driven nature of airlift circulation, for which Fr states the inertial-to-gravitational balance; it is presented here as the most indicative criterion rather than a proven controlling one. The Reynolds number remains in the fully turbulent range (10^4–10^5) at both scales, indicating that the performance loss is not caused by a flow-regime transition, and the higher P/V of the larger reactor shows that greater energy input per unit volume does not restore hydrodynamic similarity and that compensating through increased aeration carries a growing energy penalty. Establishing the causal ranking of these criteria would require experiments at three or more scales to decouple the parameter groups, which is identified as future work.

Table 3 shows the cross-scale comparison of dimensionless and energy-based scale-up parameters in the superficial gas velocity values of 0.025 and 0.1 m.s^{-1}.

Table 3.
Cross-scale comparison of dimensionless and energy-based scale-up parameters ($\boldsymbol{U_{sg}}$ = 0.025 and 0.10 m.s^{-1})

Parameter	Small reactor	Large reactor	Large/small ratio
Re	$8.7\times10^3 – 3.5\times10^4$	$2.1\times10^4 – 8.5\times10^4$	2.43
Fr	$1.8\times10^{-4} – 2.9\times10^{-3}$	$7.5\times10^{-5} – 1.2\times10^{-3}$	0.41
P/V (W.m^{-3})	8.1 – 32.6	19.3 – 77.3	2.37

4. Conclusion

This study investigated the scale-dependent hydrodynamic and gas–liquid mass transfer behavior of airlift reactors using CFD simulations at small and large reactors. The results showed that increasing superficial gas velocity improved gas holdup, gas-phase transport, and volumetric mass transfer, however, identical U_{sg} values did not preserve hydrodynamic similarity during scale-up. In the common operating range of 0.025 – 0.1 $m.s^{-1}$, the overall gas holdup in the small airlift reactor increased from approximately 0.0045 to 0.0116, whereas the corresponding values in the large airlift reactor increased only from approximately 0.0011 to 0.0026. Therefore, the small reactor maintained nearly four to five times higher gas holdup than the large reactor at identical superficial gas velocities. The air volume fraction and velocity contours confirmed that the gas phase was mainly concentrated in the riser region, but the large reactor developed a narrower and more localized gas cloud, indicating weaker radial gas dispersion and reduced gas retention. Although the average air velocity increased from approximately 0.124 to 0.141 $m.s^{-1}$ in the small reactor and from approximately 0.095 to 0.130 $m.s^{-1}$ in the large reactor, the difference between the two scales was less pronounced than that observed for gas holdup, suggesting that the lower gas holdup in the large reactor was mainly connected to the gas distribution and residence rather than upward gas velocity alone. The volumetric mass transfer coefficient also showed strong scale dependence, increasing from approximately 0.16 to 0.26 s^{-1} in the small reactor, but only from approximately 0.057 to 0.075 s^{-1} in the large reactor over the same U_{sg} range. This reduction in k_La was due to the lower gas holdup and more confined gas–liquid contact region in the larger reactor. Additional simulations for the large reactor over a wide range of aeration showed that increasing U_{sg} could partially balance the reduced performance, with gas holdup reaching approximately 0.013, k_La increasing to about 0.187 s^{-1}, and average air velocity reaching approximately 0.19 $m.s^{-1}$. Nevertheless, the response became less proportional at higher gas velocities, suggesting declining hydrodynamic and mass-transfer benefits with further aeration. The scale-up analysis based on Re, Fr, and P/V further showed that superficial gas velocity alone is not a sufficient scale-up criterion, because inertial, buoyancy-related, and energy-input effects varied differently between reactor scales. These results have several practical implications for the scale-up and design of airlift photobioreactors. First, because keeping the superficial gas velocity did not maintain the gas holdup or k_La, scale up should be based on a target mass transfer performance (gas holdup or k_La) rather than on a fixed U_{sg}. Second, although increasing U_{sg} partially recovered the performance of the larger reactor, the gains diminished at higher aeration and were accompanied by a rising power input per unit volume; raising the gas flow rate is therefore an inefficient stand-alone compensation strategy. Third, since the lower performance of the larger reactor originated mainly from the gas confinement associated with an unscaled sparger footprint, the most effective design levers are geometric, increasing the sparger area and improving its distribution, adjusting the riser cross section, and optimizing baffle spacing, so as to restore radial gas dispersion and gas-liquid contact at larger scales. Finally, the conservation of the Froude number offers a simple and physically meaningful check of buoyancy-driven similarity during initial design. These guidelines are drawn from CFD and are intended to inform and help the target scale during experimental operation. The findings indicate that scale-up of open-tube airlift photobioreactors should be guided by combined hydrodynamic, mass-transfer, and energy-based criteria, including the gas holdup, gas residence, gas-phase distribution,

k_La, Froude number, and power input per unit volume, rather than relying solely on maintaining identical superficial gas velocity.

List of Symbols

U_{sg}	Superficial gas velocity [m.s^{-1}]
ε_g	Gas holdup [-]
k_La	Volumetric mass transfer coefficient[s^{-1}]
Re	Reynolds number [-]
Fr	Froude number [-]
P/*V*	Power input per unit volume [W.m^{-3}]
Greek symbols	
ρ	Density [kg.m^{-3}]
μ	Dynamic viscosity [Pa.s]
Subscripts	
sg	Superficial gas
g	gas
l	liquid
Abbreviations	
PBR	Photo bioreactor
ALR	Airlift reactor
ALRPBR	Airlift photo bioreactor

Author Contributions

The contributions of each individual author are:

Mir Mehrshad Emamshoushtari: Investigation, Conducting formal analysis, writing—original draft preparation, writing, reviewing and editing, visualization

Farshid Pajoum Shariati: writing, reviewing and editing, supervision, project administration

Omid Tavakoli: writing, reviewing and editing, supervision, project administration

Michael Harasek: supervision, project administration

Bahram Haddadi Sisakht: supervision, project administration

Data Availability Statement

Not applicable

Acknowledgements

The authors would like to thank Mr. Salar Helchi for his support of this project.

Funding

This research did not receive any specific grant from funding agencies in the public, commercial, or not-for-profit sectors.

Conflict of interest

The authors declare no conflict of interest.

References

[1] Abdur Razzak S, Bahar K, Islam KMO, et al (2024) Microalgae cultivation in photobioreactors: sustainable solutions for a greener future. Green Chemical Engineering 5:418–439. https://doi.org/10.1016/j.gce.2023.10.004

[2] Rezvani F, Rostami K (2023) Photobioreactors for utility-scale applications: effect of gas–liquid mass transfer coefficient and other critical parameters. Environ Sci Pollut Res 30:76263–76282. https://doi.org/10.1007/s11356-023-27644-4

[3] Deprá MC, Dias RR, Zepka LQ, Jacob-Lopes E (2024) Tackling Old Challenges in Microalgal Biotechnology: The Role of Photobioreactors to Advance the Technology Readiness Level. Processes 13:51. https://doi.org/10.3390/pr13010051

[4] Uyar B, Ali MD, Uyar GEO (2024) Design parameters comparison of bubble column, airlift and stirred tank photobioreactors for microalgae production. Bioprocess Biosyst Eng 47:195–209.

https://doi.org/10.1007/s00449-023-02952-8

[5] Kumar K, Das D (2012) Growth characteristics of Chlorella sorokiniana in airlift and bubble column photobioreactors. Bioresource Technology 116:307–313. https://doi.org/10.1016/j.biortech.2012.03.074

[6] Prabhu H, Ravishankar CM, Ganesan A, et al (2025) Enhancing random forest model prediction of gas holdup in internal draft airlift loop contactors with genetic algorithms tuning and interpretability. Sci Rep 15:9325. https://doi.org/10.1038/s41598-025-92728-9

[7] Merchuk JC, Gluz M (1999) Bioreactors, Air-lift Reactors. In: Flickinger MC, Drew SW (eds) Encyclopedia of Bioprocess Technology: Fermentation, Biocatalysis, and Bioseparation. Wiley, New York, pp 320–353

[8] Xu X, Zhang Y (2023) Hydrodynamics and Mass Transfer in an Airlift Loop Reactor: Comparison between Using Two Kinds of Spargers. Processes 12:35. https://doi.org/10.3390/pr12010035

[9] Zarei Z, Malekshahi P, Trzcinski AP, Morowvat MH (2022) Investigation of Hydrodynamic Parameters in an Airlift Photobioreactor on CO2 Biofixation by Spirulina sp. Sustainability 14:7503. https://doi.org/10.3390/su14127503

[10] (2014) CFD simulation of multiphase flow in an airlift column photobioreactor. Global NEST Journal 16:1121–1134. https://doi.org/10.30955/gnj.001478

[11] Ding N, Li C, Wang T, et al (2021) Evaluation of an enclosed air-lift photobioreactor (ALPBR) for biomass and lipid biosynthesis of microalgal cells grown under fluid-induced shear stress. Biotechnology & Biotechnological Equipment 35:139–149. https://doi.org/10.1080/13102818.2020.1856717

[12] Shi J, Guo K, Wang Z, et al (2021) Computational Fluid Dynamics Simulation of Hydrodynamics in a Two-Stage Internal Loop Airlift Reactor with Contraction-Expansion Guide Vane. ACS Omega 6:6981–6995. https://doi.org/10.1021/acsomega.0c06277

[13] Amanna B, Bahri PA, Moheimani NR (2024) Application of computational fluid dynamics in optimizing microalgal photobioreactors. Algal Research 83:103718. https://doi.org/10.1016/j.algal.2024.103718

[14] Davarnejad R (2012) CFD Simulation of Scale Influence on the Hydrodynamics of an Internal Loop Airlift Reactor. ENG 04:668–674. https://doi.org/10.4236/eng.2012.410085

[15] Benyahia F, Jones L (1997) Scale Effects on Hydrodynamic and Mass Transfer Characteristics of External Loop Airlift Reactors. J Chem Technol Biotechnol 69:301–308. https://doi.org/10.1002/(SICI)1097-4660(199707)69:3%3C301::AID-JCTB716%3E3.0.CO;2-Z

[16] Juraščík M, Blažej M, Annus J, Markoš J (2006) Experimental measurements of volumetric mass transfer coefficient by the dynamic pressure-step method in internal loop airlift reactors of different scale. Chemical Engineering Journal 125:81–87. https://doi.org/10.1016/j.cej.2006.08.013

[17] Ndiaye M, Gadoin E, Gentric C (2018) CO 2 gas–liquid mass transfer and k L a estimation: Numerical investigation in the context of airlift photobioreactor scale-up. Chemical Engineering Research and Design 133:90–102.

https://doi.org/10.1016/j.cherd.2018.03.001

[18] Gouveia E, Hokka C, Badino-Jr A (2003) The effects of geometry and operational conditions on gas holdup, liquid circulation and mass transfer in an airlift reactor. Brazilian Journal of Chemical Engineering 20:363–374

[19] Blažej M, Kiša M, Markoš J (2004) Scale influence on the hydrodynamics of an internal loop airlift reactor. Chemical Engineering and Processing: Process Intensification 43:1519–1527. https://doi.org/10.1016/j.cep.2004.02.003

[20] Calvo F, Bula A, Di Mare L, Garcia S (2017) CFD simulation of multiphase (liquid–solid–gas) flow in an airlift column photobioreactor. Acta Mech 228:2413–2427. https://doi.org/10.1007/s00707-017-1828-1

[21] Korpijarvi J, Oinas P, Reunanen J (1999) Hydrodynamics and mass transfer in an airlift reactor. Chemical Engineering Science 54:2255–2262. https://doi.org/10.1016/S0009-2509(98)00439-4

[22] Koide K, Kurematsu K, Iwamoto S, et al (1983) Gas holdup and volumetric liquid-phase mass transfer coefficient in bubble column with draught tube and with gas dispersion into tube. J Chem Eng Japan / JCEJ 16:413–419. https://doi.org/10.1252/jcej.16.413

[23] Van Baten JM, Krishna R (2003) Comparison of Hydrodynamics and Mass Transfer in Airlift and Bubble Column Reactors Using CFD. Chem Eng & Technol 26:1074–1079. https://doi.org/10.1002/ceat.200301796

[24] Liew SY, Lam ZY, Gimbun J (2017) Experimental measurement and CFD simulation on the hydrodynamics of an internal-loop airlift reactor. MATEC Web Conf 111:01002. https://doi.org/10.1051/matecconf/201711101002

[25] Jasim M, Mohammed T, Sabri L (2022) Air-lift Reactor's Characterization via Computational Fluid Dynamic (CFD): Review. ETJ 40:484–497. https://doi.org/10.30684/etj.v40i3.2261

[26] Emamshoushtari MM, Tavakoli O, Harasek M, et al (2026) CFD–experimental assessment of open-tube airlift photobioreactors for CO_2 capture and nutrient removal. Journal of Environmental Chemical Engineering 14:120533. https://doi.org/10.1016/j.jece.2025.120533

[27] Yu Z, Yue S, Cheng J, et al (2026) CFD-guided optimization of a multi-hole cap for hydrodynamic intensification in an internal-loop airlift bioreactor treating refined soybean oil wastewater. Food and Bioproducts Processing 158:247–258. https://doi.org/10.1016/j.fbp.2026.05.011

[28] Grace J, Wilson J (1976) The Boundary Layer over a Populus Leaf. J Exp Bot 27:231–241. https://doi.org/10.1093/jxb/27.2.231

[29] Drew DA, Lahey RT (1987) The virtual mass and lift force on a sphere in rotating and straining inviscid flow. International Journal of Multiphase Flow 13:113–121. https://doi.org/10.1016/0301-9322(87)90011-5

[30] Tomiyama A, Tamai H, Zun I, Hosokawa S (2002) Transverse migration of single bubbles in simple shear flows. Chemical Engineering Science 57:1849–1858. https://doi.org/10.1016/S0009-2509(02)00085-4

[31] Xu L, Liu R, Wang F, Liu C-Z (2012) Development of a draft-tube airlift bioreactor for Botryococcus braunii with an

optimized inner structure using computational fluid dynamics. Bioresource Technology 119:300–305. https://doi.org/10.1016/j.biortech.2012.05.123

[32] Luo H-P, Al-Dahhan MH (2010) Local gas holdup in a draft tube airlift bioreactor. Chemical Engineering Science 65:4503–4510. https://doi.org/10.1016/j.ces.2010.04.037

[33] Merchuk JC, Garcia Camacho F (2010) Bioreactors: Airlift Reactors. In: Encyclopedia of Industrial Biotechnology, 1st ed. Wiley, pp 887–953

[34] Abashar ME, Narsingh U, Rouillard AE, Judd R (1998) Hydrodynamic Flow Regimes, Gas Holdup, and Liquid Circulation in Airlift Reactors. Ind Eng Chem Res 37:1251–1259. https://doi.org/10.1021/ie9704612

[35] Blažej M, Annus J, Markoš J (2004) Comparison of Gassing-out and Pressure-step Dynamic Methods for kLa Measurement in an Airlift Reactor with Internal Loop. Chemical Engineering Research and Design 82:1375–1382. https://doi.org/10.1205/cerd.82.10.1375.46737

[36] Zhang X, Guo K, Qi W, Zhang T, Liu C (2017) Gas holdup, bubble behaviour, and mass transfer characteristics in a two-stage internal loop airlift reactor with different screens. Can J Chem Eng 95:1202–1212. https://doi.org/10.1002/cjce.22767

[37] Ayazi Shamlou P, Pollard DJ, Ison AP (1995) Volumetric mass transfer coefficient in concentric-tube airlift bioreactors. Chem Eng Sci 50:1579–1590. https://doi.org/10.1016/0009-2509(94)00517-6.